A Storage-Based Multiagent Regulation Framework for Smart Grid Resilience

Abdallah Farraj, *Senior Member, IEEE*, Eman Hammad, *Student Member, IEEE*, and Deepa Kundur, *Fellow, IEEE*

***Abstract*—A novel framework for the distributed control is proposed in this paper for transient stability of smart power transmission systems in the face of disturbances. The proposed framework seamlessly integrates the traditional governor-based power control with energy storage system (ESS)-based controls. The design objectives also address practical challenges unaccounted for in former work, including limited ESS capacity and availability, and absent, delayed, or corrupt sensor measurements. The IEEE 68-bus test power system is used to demonstrate the merits of the control strategy in enhancing the transient stability of power systems. The results of this paper suggest that integrating different types of control can lead to an enhanced transient stabilization process in the face of different practical limitations.**

***Index Terms*—Distributed control, energy storage system (ESS), feedback linearization, smart grid resilience, transient stability.**

I. Introduction

INTEGRATION of advanced sensors and cyber-enabled control can greatly enhance the performance and resiliency of power systems by facilitating distributed optimization and control [1]–[6]. This is largely enabled through the communication network connectivity between power system sensors and control centers. Moreover, there is steady growth in the adoption of energy storage systems (ESSs) for power system applications. These advancements motivate the integration of new informed distributed ESS-based control paradigms in the evolving "smart" grid including at the power transmission system level. The power transmission grid consists, in part, of synchronous machines that represent an essential power generation backbone such that the system is considered stable if these synchronous machines return to a stable steady-state operating point after the occurrence of a disturbance [7].

Transient stability studies are concerned with the ability of the power system to maintain synchronism when subjected to a severe disturbance such as loss of generation units, faults, and cyber attacks. Transient stability depends on the ability of the synchronous generators to maintain or restore a balance between their electromechanical and mechanical torques. If a power system exhibits transient instability, some synchronous generators may experience increasing angular swings leading to loss of synchronism between the different generators. For complex power systems, transient stability studies are typically carried out through numerical simulation.

It is well known that vulnerabilities exist at the intersection of communication networks and physical systems [8]; hence, the cyber enablement of power systems exposes them to new weaknesses. For instance, the use of insecure communication links can allow for cyber attacks that damage smart grid operation [9]. Attacks on information availability often manifest as denial-of-service (DoS) targeting communication channels where an adversary interrupts the operation of a communication component, which leads to excessive delays in information exchange [10]. In attacks on data integrity, an adversary manipulates the structure of the data delivery system by means of false data injection (FDI) to introduce stealthy errors in data while bypassing bad data detection filters [11].

Recent distributed control work has capitalized on the cyber-physical smart grid paradigm by proposing schemes for transient stability. For example, the authors in [5] and [12]–[25] study the impact of control activation in restoring the power system stability. Some proposed controllers, designed under ideal conditions, actuate distributed ESSs to inject and/or absorb power from the grid to change the power system dynamics and achieve stability. However, several practical issues still limit the performance of these ESS-based distributed control schemes. For example, the absence of ESSs at generator buses, ESSs with limited inject/absorb capacity, unreliable sensor readings, and high latency between sensors and controllers are some examples of scenarios that restrict performance. FDI attacks on measurements, DoS attacks on communication nodes, and interference can also hinder the distributed controllers' performance.

Resilient power systems reduce the magnitude and/or duration of service disruption during disturbances. In this paper, a *Storage-Based Multiagent Regulation* framework is proposed to harness the growth in ESSs in order to enhance the smart grid resilience and to aid in transient stability under a number of practical conditions unaddressed by existing work. The proposed control framework seamlessly integrates and co-ordinates the operation of the traditional governor-based control with

Manuscript received July 27, 2017; revised September 29, 2017 and November 7, 2017; accepted December 14, 2017. Date of publication January 4, 2018; date of current version September 4, 2018. Paper no. TII-17-1651. *(Corresponding author: Abdallah Farraj.)*

The authors are with the Department of Electrical and Computer Engineering, University of Toronto, Toronto, ON M5S 3G4, Canada (e-mail: abdallah@ece.utoronto.ca; ehammad@ece.utoronto.ca; dkundur@ece.utoronto.ca).

Color versions of one or more of the figures in this paper are available online at http://ieeexplore.ieee.org.

Digital Object Identifier 10.1109/TII.2018.2789448

storage-based controls. The control framework also aims to simultaneously address both cyber and physical disturbances in the power system; the control scheme is designed to be resilient to changes and constraints in cyber and physical environments by adapting its structure and/or parameters to reflect limitations in connectivity and storage. Furthermore, in contrast to the existing work, the proposed control framework addresses the following critical practical issues:

1) insufficient capacity or absent ESS;
2) limited or lost communication connectivity;
3) measurements that are absent, severely delayed, or corrupted by noise or interference;
4) a distributed controller without an associated sensor.

The remainder of this paper is organized as follows. The problem setting is presented in Section II. Sections III and IV present the proposed framework. Section V numerically investigates the performance of the control framework. Finally, conclusions and final remarks are in Section VI.

II. Distributed Control for the Transient Stability

We summarize the transient stability problem in power systems and introduce a multiagent representation for smart grids followed by a description of control agents. We then formulate storage-based distributed control for the transient stability.

A. Problem Formulation

In this paper, we aim to lay a foundation for a control framework for transient stability applications. One main goal of the proposed framework is to strengthen the power grid's resilience to cyber and physical disturbances through reactive distributed control approaches. The design and development objectives include the followings:

1) incorporating a multiagent paradigm for smart grids that represents a scalable and resilient topology for cyber-physical operation;
2) stabilizing the power grid after the onset of physical disturbances;
3) integrating different forms of control for flexibility;
4) reducing the operational time and control power of ESSs during the stabilization process by incorporating mechanical power control;
5) responding adaptively to changing cyber connectivity and storage capacity.

The control framework addresses reasonable practical limitations including when an ESS has limited inject/absorb capacity or is absent (which translates to zero capacity), limited communication connectivity, an absent sensor, and delayed or corrupted measurements due to noise or interference.

The proposed control framework should enhance the smart grid resilience by improving the ability of the power system to absorb, adapt to, and recover from cyber and physical disturbances. The power system coping capability is improved as a result of the application of storage-based and mechanical power-based control schemes, the reactive nature of the control framework to connectivity and delay in the cyber network, and the control adaptability to storage constraints and sensor availability.

TABLE I
Machine Model Parameters

Parameter	Description
δ	Rotor angle
ω	Rotor angular speed
ω_s	Synchronous speed
D	Damping coefficient
E'_d	d-axis transient electromotive force (emf)
E'_q	q-axis transient emf
E_f	Field voltage
H	Machine inertia constant
I_d	d-axis component of the stator current
I_q	q-axis component of the stator current
R_a	Armature resistance
X_d	d-axis synchronous reactance
X_q	q-axis synchronous reactance
X'_d	d-axis transient reactance
X'_q	q-axis transient reactance
T'_d	d-axis transient open-loop time constant
T'_q	q-axis transient open-loop time constant
T_E	Electromechanical torque
T_M	Mechanical torque
V_d	d-axis terminal voltage
V_q	q-axis terminal voltage

B. Power System Transient Dynamics

Consider a power transmission system that is comprised of N synchronous generators with generator parameters defined in Table I. For generator i $\forall i \in \{1, \ldots, N\}$, the widely used two-axis subtransient machine model is employed to capture the dynamics of the synchronous generator during transients. Let $\dot{E}'_{qi}$ and $\dot{E}'_{di}$ denote the time derivatives of E'_{qi} and E'_{di}, respectively, then the electrical dynamics of generator i's stator are given by [26], [27]

$$\dot{E}'_{qi} = \frac{1}{T'_{di}}\left(-E'_{qi} - (X_{di} - X'_{di})I_{di} + E_{fi}\right) \tag{1}$$

$$\dot{E}'_{di} = \frac{1}{T'_{qi}}\left(-E'_{di} + (X_{qi} - X'_{qi})I_{qi}\right) \tag{2}$$

$$E'_{qi} = V_{qi} + R_{ai}I_{qi} + X'_{di}I_{di} \tag{3}$$

$$E'_{di} = V_{di} + R_{ai}I_{di} - X'_{qi}I_{qi}\,. \tag{4}$$

Let Ω_s denote the system frequency (typically equal to $60 \cdot 2\pi$ or $50 \cdot 2\pi$ [rad/s] depending on the geographical area). The swing equation describes the rotor dynamics of the synchronous generator captured by [26]

$$\dot{\delta}_i = \Omega_s(\omega_i - \omega_s) \tag{5}$$

$$\dot{\omega}_i = \frac{\omega_s}{2H_i}\left(T_{Mi} - T_{Ei} - D_i(\omega_i - \omega_s)\right) \tag{6}$$

where $\dot{\delta}_i$ and $\dot{\omega}_i$ denote the time derivatives of δ_i and ω_i, respectively. The swing equation describes the electromechanical dynamics of a synchronous generator's rotor, and is thus useful for studying a generator's behavior during a large disturbance.

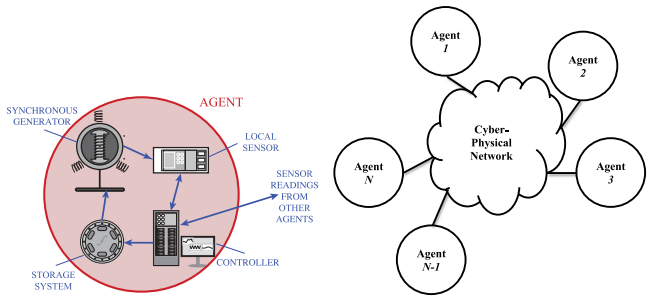

Fig. 1. Multiagent cyber-physical representation of the smart grid. (a) Cyber-physical agent. (b) Cyber-physical system.

In this model, the field voltage of a synchronous generator is controlled by the excitation system, input mechanical torque is controlled by the speed governor, and output electromechanical torque is calculated using [26]

$$T_{Ei} = E'_{di} I_{di} + E'_{qi} I_{qi} + (X'_{qi} - X'_{di}) I_{di} I_{qi} \tag{7}$$

which provides a nonlinear term in (6). Let P_{Mi} and P_{Ei} denote the mechanical and electrical powers of generator i, respectively, where $P_{Ei} = T_{Ei}$ and $P_{Mi} = T_{Mi}$ when employing per units. Also, let $P_{Ai} = P_{Mi} - P_{Ei}$ refer to the accelerating power of generator i. Typically, $P_{Ai} = 0$ during normal power system operation. However, when a major system disturbance occurs, the accelerating power of a subset of generators can deviate from 0. In this case, a generator's rotor will increase (decrease) its speed when P_{Ai} is positive (negative). A large deviation in the rotor speed might damage the synchronous machine; consequently, a generator might be disconnected from the grid to prevent damage.

C. Smart Grid Multiagent Representation

The smart grid is modeled as a multiagent cyber-physical system comprised of N agents as depicted in Fig. 1. In this representation, cyber-physical agent i includes a synchronous generator i and may possibly consist of the followings:

1) an associated sensor that provides local measurements of the generator rotor angle δ_i, rotor speed ω_i, and internal voltage E_i;
2) communication transceivers to connect different smart grid agents for the transmission of δ_i, ω_i, and E_i;
3) a controller that processes sensor data from system agents and calculates control signals u_i and v_i that affect the dynamics of the power system by utilizing
    1) a fast-acting ESS that can inject or absorb real power at the bus of generator i depending on the value of the associated control signal u_i;
    2) a mechanical power control to possibly change P_{Mi} (by regulating the speed governor) depending on the value of control signal v_i.

The physical dynamics of each cyber-physical agent depend on its own (synchronous generator) state and the states of other agents in the power system. In this modeling, the different agents are connected through the *cyber-physical network* that includes the physical power system and the associated cyber communication system. The physical connectivity between the agents is a result of the transmission lines and physical dynamics of the power system in (1)–(6), while the cyber-enabled control and communication systems lead to cyber connectivity.

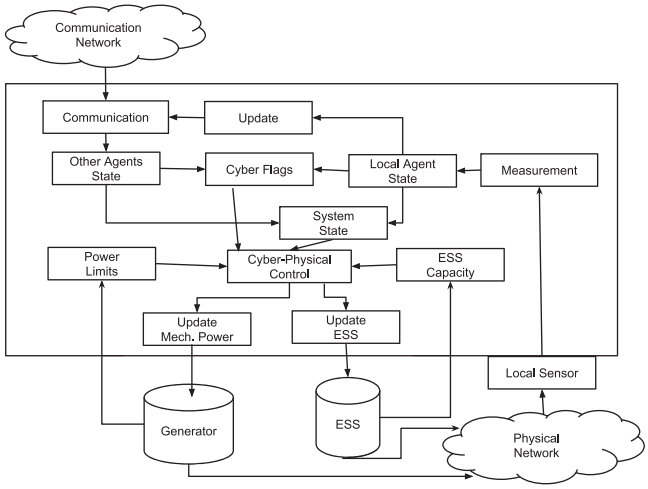

Fig. 2. Logical modules of a control agent.

The controller (a.k.a. control agent) affects the power system dynamics by actuating the local ESS, if present, through u_i and regulating the governor of its associated generator to affect the input mechanical power through v_i. The control agent computes control signals from sensor readings received locally and through the communication network, and the control action is adaptive to changing cyber and physical environments and constraints.

As shown in Fig. 2, a control agent has the following logical modules. The measurements module acquires sensor readings, typically in the form of periodic measurements of phasor voltage and current values near the generator bus that are sampled, quantized, and then, coded into bits. The system state module estimates the generator rotor speed (by, for example, estimating the zero crossings of current or voltage measurements), rotor angle (by integrating the rotor speed signal), and accelerating power [by, for example, calculating (7)]. The flags module labels any corrupted measurement with the appropriate flags (e.g., levels of noise or latency). The update module saves the local generator's rotor speed and angle values, along with other system metrics such as latency and noise levels to a shared memory location accessible to other modules after formatting.

The communication module transmits (receives) local state information to (from) other agents and reads (writes) from (into) the local shared memory. The local rotor speed and angle values are encoded according to the communication standard and sent over the communication network via, for example, fiber optics, wireless communications, or satellite communications links. The control module computes the control signal using system state variables, latency, noise levels, and other flags. Following two types of control signals are generated:

1) u_i to regulate the output of the local ESS, and this component checks the charging level of the ESS and limits the control signal accordingly;

2) v_i to regulate the input mechanical power of the generator, and this component limits the control signal value to the power limits of the speed governor.

In this model, full cyber connectivity enables agents to calculate the mismatch between electrical and mechanical powers during transients. For example, agent i uses its sensors to acquire the local measurements of the generator's rotor angle δ_i, rotor speed ω_i, and internal voltage E_i. Then, the communication transceiver of the agent connects with the other smart grid agents to exchange the values of δ_i, ω_i, and E_i. Once agent i acquires these measurements from the other agents, the electrical power of agent i is calculated using [28]

$$P_{Ei} = \sum_{k=1}^{N} |E_i||E_k| \left(G_{ik}\cos\left(\delta_i - \delta_k\right) + B_{ik}\sin\left(\delta_i - \delta_k\right)\right)$$

where $G_{ik} = G_{ki}$ and $B_{ik} = B_{ki}$ represent the Kron-reduced equivalent conductance and susceptance between generators i and k, respectively. After P_{Ei} is calculated, the value of P_{Ai} can be determined for agent i. The availability of P_{Ai} can enable control agents to employ aggressive forms of control as will be shown in Section III.

D. Distributed Control Paradigm

An ESS is a device that is used to store energy, which can be injected in the power system for a variety of objectives; such device has the ability to respond to load variations and control signals by injecting or absorbing power [20]. There are different types of ESSs, including mechanical, electrical, thermal, biological, and chemical systems. Popular ESS technologies include flywheels, pumped hydro, solid state, compressed air, and capacitor systems. As power systems transform into smarter grids, ESSs can help in maintaining the system stability and reliability.

Distributed control is considered for stabilizing a smart grid under major disturbances. The focus in this paper is on a control scheme that leverages ESS devices to absorb and inject power at a variety of locations to "shape" the power system dynamics and promote transient stability. Effective control of ESSs relies on the exchange of sensor readings through communication channels to compute the control vectors that determine the level of power injection or absorption. The case in which an ESS interfaces with the smart grid at the bus of generator i with associated control u_i is considered. The swing equation of generator i with integrated ESS-based control of u_i can be described at time t as

$$\begin{aligned}\dot{\delta}_i(t) &= \Omega_s(\omega_i(t) - \omega_s)\\ \dot{\omega}_i(t) &= \frac{\omega_s}{2H_i}\left(P_{Ai}(t) - D_i(\omega_i(t) - \omega_s) + u_i(t)\right). \end{aligned} \quad (8)$$

Several control strategies can be used to calculate u_i including linear and nonlinear schemes. In this relation, u_i provides a generic form of control; also, the specific inertia and characteristics of the storage device affect the rate of change of power injection/absorption at any given moment.

III. Storage-Based Multiagent Regulation Framework

The "storage-based multiagent regulation" framework for transient stability is detailed in this section. The storage and mechanical control components are explained, and a stability study is conducted.

A. Framework Overview

The proposed control framework integrates storage-based and mechanical-based distributed controls and addresses practical issues in the distributed smart grid control as outlined in Section II. The proposed framework considers different degrees of communication network connectivity and ESS and measurement availability. The mechanical power control has to change the input mechanical torque slowly. Thus, the ESS-based control (if available) is proposed to start first; as the ESS control stabilizes the rotor speed, the mechanical power control component is activated to close the gap in accelerating power and to allow the output of the ESS to go to zero while keeping the synchronous generators stable. It is to be noted here that the proposed control framework does not replace existing power control schemes (such as power system stabilizers and exciting systems); on the contrary, the proposed framework complements and enhances those control methods.

For transient stability studies, a synchronous generator is said to be stabilized if its rotor speed is driven back to an acceptable range and when synchronism with other generators is restored. Hence, one goal of the proposed control scheme is to regain a balance between the mechanical and electromechanical torques of the synchronous generators; this leads to constant rotor speeds that restore synchronism between the system generators and drive rotor speeds to an acceptable range. Specifically, a generator is denoted stable in this paper if its rotor speed is between 59.8 and 60.2 Hz [29] (i.e., 0.9967 p.u. $\leq \omega \leq$ 1.0033 p.u.); otherwise, the generator is classified as unstable. In this context, stability time refers to the time it takes the control scheme to stabilize the synchronous generators of the power system.

B. Storage-Based Control

ESS-based control (u_i) affects the operation of the associated storage device to achieve the transient stability; a positive (negative) u_i value in (8) indicates that the ESS injects (absorbs) real power from the bus of generator i. Let the capacity of the ESS of agent i at time t be denoted $C_i(t)$. Then, to account for capacity limits of the local storage device, u_i is given by

$$u_i(t) = \begin{cases} C_i(t) & \hat{u}_i(t) > C_i(t) \\ \hat{u}_i(t) & -C_i(t) \leq \hat{u}_i(t) \leq C_i(t) \\ -C_i(t) & \hat{u}_i(t) < -C_i(t) \end{cases} \quad (9)$$

where $\hat{u}_i$ is the parametric feedback linearization (PFL) control signal computed using [30]

$$\hat{u}_i(t) = -P_{Ai}(t) - \alpha_i(\omega_i(t) - \omega_s). \quad (10)$$

Through the design parameter $\alpha_i \geq 0$, the PFL control signal reshapes the dynamics of the closed-loop power system as a series of stable linear systems with tunable eigenvalues.

Once $\hat{u}_i$ is calculated, the ESS-based control component actuates the associated ESS according to (9). As the generators are stabilized by the ESS-based control (i.e., $|\omega_i - \omega_s| \leq 0.0033$ p.u.), the mechanical power control (discussed next) is activated in order to close the accelerating power gap. Specifically, the v_i control signal slowly adjusts the input mechanical power of generator i, and the magnitude of u_i is correspondingly reduced as $|P_{Ai}|$ approaches zero. Finally, when $P_{Ai} = 0$, the mechanical power control component stops adjusting T_{Ei} while leaving the power system stable.

An ESS with a small capacity limit increases the time-to-stability for the ESS-based control component. Consequently, the v_i control component can start before the generator achieves stability; however, the control coefficients have to be chosen small enough in order to reduce the fluctuations in the input mechanical power.

C. Mechanical Power Control

A successful ESS-based control brings the rotor speeds to an acceptable range yet the gap between mechanical and electromechanical torques remains unaddressed. The mechanical power is usually varied by the speed governor in response to changes in the rotor speed; however, such changes are typically slow. Also, given that the rotor speed is stabilized by the ESS-based control, the governor control is not guaranteed to start changing the value of T_{Mi} in a timely manner. Hence, the mechanical power control v_i is proposed to slowly change the input mechanical power (P_{Mi}) in order to close the gap with P_{Ei} allowing u_i to approach zero while maintaining the transient stability. The v_i control component also accommodates the cases of an ESS with insufficiently small inject/absorb capacity or a generator bus without any associated ESS. This type of control is necessarily restricted to exhibit a low rate of change to avoid equipment damage when applied to the speed governor. The reader should note that v_i control works at a larger timescale than u_i control, but it is quicker than the traditional speed governor control, which it enhances.

Let $\hat{v}_i(t) = P_{Mi}(t) - P_{Ei}(t)$, which is the accelerating power of generator i at time t. After activation, the v_i control signal is proposed to exhibit the following dynamics:

$$\dot{\hat{v}}_i = -\gamma_i \hat{v}_i \tag{11}$$

where $\dot{\hat{v}}_i$ is the time derivative of $\hat{v}_i$ and $\gamma_i \geq 0$ is a design parameter. A small positive value of γ_i is desired as it slows down the rate of change in P_{Mi}. After control activation, the time-domain representation of $\hat{v}_i$ is

$$\hat{v}_i(t) = \hat{v}_i(t_v) e^{-\gamma_i (t - t_v)} \tag{12}$$

where t_v is the time when the mechanical power control component is activated and $\hat{v}_i(t_v)$ is equal to the accelerating power at that moment. Thus, the preprocessed control signal, denoted $\hat{P}_{Mi}$, is found as $\hat{P}_{Mi}(t) = \hat{v}_i(t) + P_{Ei}(t)$ for time $t \geq t_v$. Consequently, $\hat{P}_{Mi}$ is calculated according to

$$\hat{P}_{Mi}(t) = \begin{cases} P_{Mi} & t < t_v \\ P_{Ei}(t) + P_{Ai}(t_v) e^{-\gamma_i (t - t_v)} & t \geq t_v \,. \end{cases} \tag{13}$$

Let the maximum and minimum mechanical power values that can be injected into generator i be denoted $P_{i,\max}$ and $P_{i,\min}$, respectively. The v_i control signal that will be applied to the governor of generator i is calculated as

$$v_i(t) = \begin{cases} P_{i,\max} & \hat{P}_{Mi}(t) > P_{i,\max} \\ \hat{P}_{Mi}(t) & P_{i,\min} \leq \hat{P}_{Mi}(t) \leq P_{i,\max} \\ P_{i,\min} & \hat{P}_{Mi}(t) < P_{i,\min} \end{cases} \tag{14}$$

where the limiter bounds the control signal from exceeding the power limits. In this manner, the input mechanical power of generator i is varied at time t according to $v_i(t)$.

If a generator is without an associated ESS, or if the ESS has an insufficient capacity, then the v_i control signal serves to slowly adjust the mechanical power of the generator to make $P_{Ai} = 0$, and thus, achieve transient stability. When a cyber-physical agent does not have an associated ESS (due to the lack of the storage device or an empty ESS), u_i control cannot be applied for that control agent. In this case, the mechanical power control scheme can aid in achieving stability by activating the v_i controller sooner. However, the v_i control coefficient γ_i must be selected small (at the early stages of v_i control activation) in order to slow down the fluctuations in the input mechanical power of the associated generator.

D. Stability Study

Let $\boldsymbol{x}_i = [\delta_i, \omega_i - \omega_s, P_{Ai}]^T$ denote the state variable of agent i. After applying the proposed control scheme in (10) and (11), the agent dynamics can be described as

$$\dot{\boldsymbol{x}}_i = \boldsymbol{A}_i \boldsymbol{x}_i \tag{15}$$

where $\dot{\boldsymbol{x}}_i$ is the time derivative of $\boldsymbol{x}_i$ and

$$\boldsymbol{A}_i = \begin{cases} \begin{bmatrix} 0 & \Omega_s & 0 \\ 0 & \frac{-\omega_s}{2H_i}(D_i + \alpha_i) & 0 \\ 0 & 0 & 0 \end{bmatrix} & \text{only } u_i \text{ control} \\ \begin{bmatrix} 0 & \Omega_s & 0 \\ 0 & \frac{-\omega_s}{2H_i} D_i & 0 \\ 0 & 0 & -\gamma_i \end{bmatrix} & \text{only } v_i \text{ control} \\ \begin{bmatrix} 0 & \Omega_s & 0 \\ 0 & \frac{-\omega_s}{2H_i}(D_i + \alpha_i) & 0 \\ 0 & 0 & -\gamma_i \end{bmatrix} & \text{both } u_i \text{ and } v_i. \end{cases} \tag{16}$$

The proposed control scheme converts the nonlinear intercoupled dynamics of the synchronous generators in (5) and (6) into a series of decoupled linear dynamics as shown previously. The nonzero eigenvalues of the controlled agent in (15) can be shown to equal $-\frac{\omega_s}{2H_i}(D_i + \alpha_i)$ for the ESS-based control, $\frac{-\omega_s}{2H_i} D_i$ and $-\gamma_i$ when the mechanical power control is only

active, and $-\frac{\omega_s}{2H_i}(D_i+\alpha_i)$ and $-\gamma_i$ when both controls are activated. Consequently, transient stability is achieved and enhanced as all nonzero eigenvalues are in the left-hand complex plane. Measurement uncertainties affect the speed of stabilization; however, stability can still be achieved if the uncertainty magnitude is bounded to some threshold [30].

It is observed that the control design parameters (α_i and γ_i) have direct impact on the nonzero eigenvalues and on agent stability. Furthermore, higher values of α_i and γ_i can speed up the stabilization process; however, a higher value of α_i usually leads to higher amounts of the ESS power, and a smaller value of γ_i is preferred to slow down the rate of change in the input mechanical power of the synchronous generators.

E. Closed-Loop Dynamics

When there is no disturbance in the power system, the values of relative rotor speed ($\omega_i-\omega_s$) and accelerating power P_{Ai} are both zero; hence, the power system is stable with no transients. Consequently, the distributed controller is inactive; i.e., $u_i(t)=0$ and $v_i(t)=P_{Mi}$, and that means the ESS does not inject (absorb) power in (from) the system and the mechanical power of generator i is not varied. When a disturbance causes the power system to deviate from its equilibrium, the relative rotor speed deviates from zero and there is a corresponding mismatch between electromechanical and mechanical torques in some generators. The objective of the control agent is to change the dynamics of the power system to achieve a stable equilibrium. Over a short time period, the proposed control scheme accomplishes this task by actuating the ESSs to inject or absorb power from the system according to a control law that facilities convergence of $\omega_i(t)-\omega_s=0$. The stabilization action can be achieved by employing available sensor readings depending on the communication architecture.

Although a successful operation of the ESS-based control brings the rotor speeds to an acceptable range, the mismatch between mechanical and electromechanical torques does not disappear. This requires the u_i control signal to stay active to supplement the power difference in order to keep the generators stable. The purpose of the v_i control component is to change the input mechanical power (at a slower timescale than u_i, but faster than typical governor control) to close the accelerating power gap allowing the output of the ESS-based control to go to zero while maintaining the power system stability.

IV. Control for Data Availability and Integrity

Practical considerations related to measurement integrity and timely availability are addressed in this section.

A. Delayed Measurement

Following the results of [31], the ESS-based control component can be made more robust to prolonged communication latency. Here, the design parameter for u_i in (10) (i.e., α_i) is piece-wise linearly varied depending on the value of communication delay between the sensors and control agents. Let τ_i denote the latency between the sensors and agent i, then the value of α_i is chosen as

$$\alpha_i(\tau_i)=\begin{cases}\alpha_{\max} & \tau_i<\tau_{\text{opt}}\\ -a\tau_i+b & \tau_{\text{opt}}\le\tau_i\le\tau_{\max}\end{cases} \tag{17}$$

where a , b, τ_{opt}, and $\tau_{\max}$ are positive parameters that depend on the power system under consideration. When τ_i is small and below a threshold τ_{opt}, α_i is selected to be maximum $\alpha_{\max}$. However, when latency increases, α_i is linearly decreased up to an upper latency limit of $\tau_{\max}$. Further, if the communication network experiences prolonged delays and τ_i exceeds $\tau_{\max}$, the ESS control can switch to a local mode of operation (described next). As previously discussed, the control parameter α directly affects the eigenvalues of the closed-loop system, and a higher value of α leads to faster stability but also to potentially higher amounts of control power. Consequently, reducing α might lead to longer stability times, resulting in delays in the activation of the v_i control.

When the network connectivity is lost or when there is an excessive delay between sensors and controllers (i.e., $\tau_i>\tau_{\max}$), a local control mode can be employed. This control mode relies on local measurements only to calculate the control signal. For example, $\hat{u}_i$ is computed in a local control mode as [32]

$$\hat{u}_i(t)=-\alpha_i(\omega_i(t)-\omega_s)\,. \tag{18}$$

After applying this local control scheme, agent i dynamics can be described as $\dot{\boldsymbol{x}}_i=\boldsymbol{A}_i\boldsymbol{x}_i$, where

$$\boldsymbol{A}_i=\begin{bmatrix}0 & \Omega_s & 0\\ 0 & \frac{-\omega_s}{2H_i}(D_i+\alpha_i) & \frac{\omega_s}{2H_i}\\ 0 & 0 & 0\end{bmatrix}.$$

The nonzero eigenvalue of $\boldsymbol{A}_i$ is $-\frac{\omega_s}{2H_i}(D_i+\alpha_i)\le 0$. Thus, applying this mode of control leads rotor speeds to converge exponentially to ω_s, guaranteeing the transient stability. However, applying (18) can result in longer stability times due to the missing accelerating power component. Thus, employing the v_i control to stabilize the power grid can also be a feasible solution when the network experiences excessive delays or when connectivity between the agents is lost.

B. Unavailable Measurement

A measurement is unavailable when a cyber-physical agent does not have a local sensor or when the measurement is severely corrupted by noise or interference (detected with the aid of the flags module). Consider a power system that is partitioned into nonoverlapping clusters (a.k.a. control areas) of cyber-physical agents, where clusters are formed based on high physical coupling between the agents. When an agent lacks its own sensor measurements, available readings from other sensors within the same cluster are utilized to calculate the control signal for that agent. Given the strong intraarea physical coupling in a cluster, the different agents are expected to share similar dynamics. Hence, the state of a generator lacking measurements is inferred from those of other generators in the same cluster.

Specifically, let area S_j include N_j agents. Assume that generator $\tilde{i}$ in this area does not have a valid measurement; consequently, the values of $\delta_{\tilde{i}}$ and $\omega_{\tilde{i}}$ are unknown to the control agent.

However, other agents in S_j have sensors, and so the values of their rotor speed and angle are known and shared with all control agents in S_j through the communication network. Define $S_{\tilde{j}}$ to be the set of all agents in S_j except Agent $\tilde{i}$ (i.e., $S_{\tilde{j}}$ has $N_j - 1$ agents). The ESS-based control signal of the different generators in area S_j can be calculated using

$$\hat{u}_i(t) = \begin{cases} -\alpha_i(\omega_i(t) - \omega_s) & i \neq \tilde{i} \\ -\alpha_i(\hat{\omega}_{\tilde{i}}(t) - \omega_s) & i = \tilde{i} \end{cases} \tag{19}$$

where

$$\hat{\omega}_{\tilde{i}}(t) = \frac{1}{N_j - 1} \sum_{k \in S_{\tilde{j}}} \omega_k(t)\,. \tag{20}$$

Thus, the control signal for each agent is determined by the available measurements from the associated control area. If the agent has its sensor readings (i.e., $i \neq \tilde{i}$), the control agent utilizes the local measurement to calculate $\hat{u}_i$; however, if the agent lacks a sensor (i.e., $i = \tilde{i}$), the average value of the known measurements in area S_j is employed when calculating the control signal. Since the agents in area S_j are strongly coupled, $\hat{\omega}_{\tilde{i}}$ should be close to the actual value of $\omega_{\tilde{i}}$.

After applying the proposed control scheme in (20) in area S_j, agent i dynamics can be described as $\dot{\boldsymbol{x}}_i = \boldsymbol{A}_i \boldsymbol{x}_i + \boldsymbol{b}_i$, where $\boldsymbol{x}_i = [\delta_i, \omega_i - \omega_s, P_{Ai}]^T$ is the associated state variable. Also

$$\boldsymbol{A}_i = \begin{bmatrix} 0 & \Omega_s & 0 \\ 0 & \frac{-\omega_s}{2H_i}(D_i + \alpha_i) & \frac{\omega_s}{2H_i} \\ 0 & 0 & 0 \end{bmatrix} \tag{21}$$

and

$$\boldsymbol{b}_i = \begin{cases} \begin{bmatrix} 0 & 0 & 0 \end{bmatrix}^T & i \neq \tilde{i} \\ \begin{bmatrix} 0 & \frac{-\omega_s}{2H_i}\alpha_i \epsilon_i & 0 \end{bmatrix}^T & i = \tilde{i} \end{cases} \tag{22}$$

where $\epsilon_{\tilde{i}}$ is the difference between the actual rotor speed of agent $\tilde{i}$ and the calculated one from the other agents in the area; i.e., $\epsilon_{\tilde{i}} = \frac{1}{N_j - 1} \sum_{k \in S_{\tilde{j}}} \omega_k - \omega_{\tilde{i}}$. The nonzero eigenvalue of $\boldsymbol{A}_i$ is $-\frac{\omega_s}{2H_i}(D_i + \alpha_i) \leq 0$. Hence, for agents with sensors, the rotor speed will converge exponentially to ω_s, guaranteeing transient stability for the case of $i \neq \tilde{i}$. This leads to $\epsilon_{\tilde{i}}$ converging to $\omega_s - \omega_{\tilde{i}}$ (i.e., making this term bounded), which will asymptotically reduce the residue in $\boldsymbol{b}_{\tilde{i}}$ to zero, and ultimately stability is achieved for the case $i = \tilde{i}$.

C. Summary of Control Operation

The operation of the proposed storage-based multiagent regulation framework is summarized in this section. The following cases are considered.

1) *Normal control operation*: Start u_i control of (10), then activate v_i control of (11) as the system starts to stabilize.
2) *Insufficient storage capacity*: Start u_i control, but activate v_i control sooner.
3) *Lost connectivity*: Activate the local control mode of (18).
4) *Unavailable storage*: Activate v_i control with small value of γ_i.

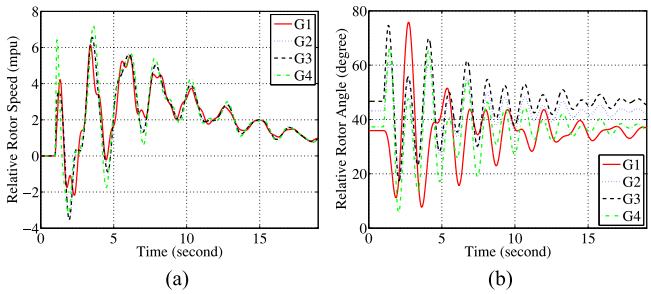

Fig. 3. Sample relative rotor speed and angle for generators $1-4$ when control is not activated. (a) Relative rotor speed. (b) Relative rotor angle.

5) *Delayed measurements*: Adapt the control scheme to latency by varying α_i as described in (17).
6) *Missing sensor or corrupted measurements*: Cluster the agents in control areas and apply the control of (19).

V. Numerical Results

Results of numerical experiments are reported in this section. The IEEE 68-bus test power system is used for simulations. The power system parameters are extracted from [33] and [34], and the simulation environment follows the guidelines in [26]. Consider standard three-phase faults at Buses 24, 27, 30, 36, 37, 54, 60, and 66. These faults start at $t = 1$ s and are cleared after five cycles. The proposed control scheme is not activated for the results of Fig. 3. The relative rotor speed $(\omega_i - \omega_s)$ for generators $1-4$ is displayed in Fig. 3(a), and Fig. 3(b) shows the relative rotor angle $\delta_i - \delta_{13}$ (using generator 13 as a reference). Both the rotor speed and the angle do not converge rapidly to stability even though the system generators are equipped with traditional power control schemes; similar results can also be found for the other system generators. Without activating the proposed control scheme, the average stability time of the test power system is about 7.07 s.

A. Operation of the Control Scheme

Fig. 4 demonstrates a sample performance when only u_i control is activated at $t = 1$ s for the same set of physical disturbances. The maximum capacity of an ESS is set to a small value of 5% of the mechanical power of the generator, and $\alpha_i = D_i$ is used. The rotor speed and angle are stabilized quickly due to the action of the u_i control. Further, as Fig. 4(c) and (d) shows, the ESS supplements the difference in the accelerating power to keep the generators stable. For the different mentioned faults, the average stability time for the u_i control is about 2.08 s. Furthermore, similar results can be found for the local control mode of (18) that can be utilized for the case of lost cyber connectivity; the average stability time for the local mode is around 3.34 s.

The effect of only activating the v_i control component at $t = 2.5$ s for $\gamma_i = 1$ is shown in Fig. 5. This scenario demonstrates the case of an unavailable storage or lost cyber connectivity. Both rotor speed and angle are stabilized rapidly. It is observed in Fig. 5(d) that the mechanical power changes over time in order

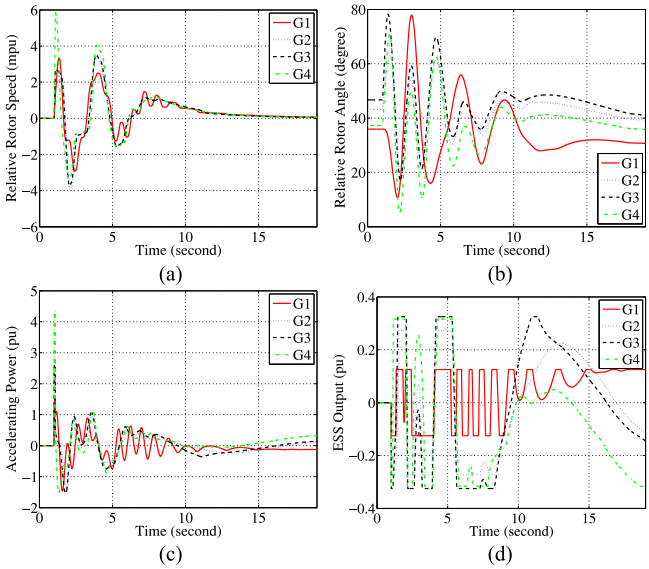

Fig. 4. Sample performance when only u_i control is activated. (a) Relative rotor speed. (b) Relative rotor angle. (c) Accelerating power. (d) ESS output.

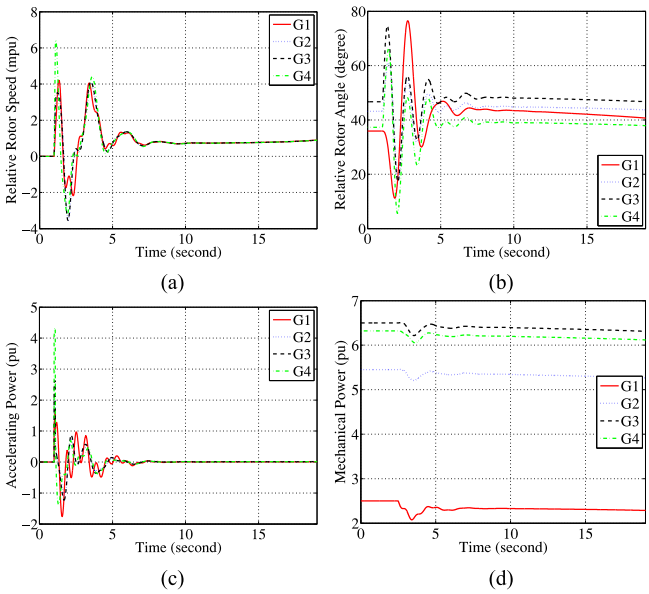

Fig. 5. Sample performance when only v_i control is activated. (a) Relative rotor speed. (b) Relative rotor angle. (c) Accelerating power. (d) Mechanical power.

to close the accelerating power gap as shown in Fig. 5(c). The generators are stabilized within about 2.27 s from the onset of the disturbance. Even though the figure does not shows that $\omega_i \to \omega_s$ in the displayed time interval, the generators are denoted as stable since $|\omega_i - \omega_s| \leq 0.0033$ pu is satisfied within few seconds from the v_i control time.

Fig. 6 presents the impact of activating both controls u_i at $t = 1$ s and v_i at $t = 2.5$ s to address the limited storage capacity. The rotor speed and angle are stabilized rapidly. As Fig. 6(c) also shows, the power contribution from the ESSs declines to zero, while the input mechanical power of the generators slowly

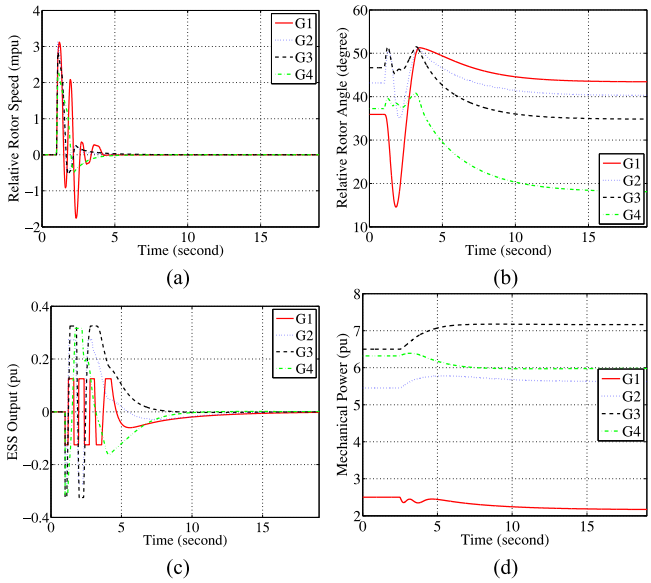

Fig. 6. Sample performance when both u_i and v_i controls are activated. (a) Relative rotor speed. (b) Relative rotor angle. (c) ESS output. (d) Mechanical power.

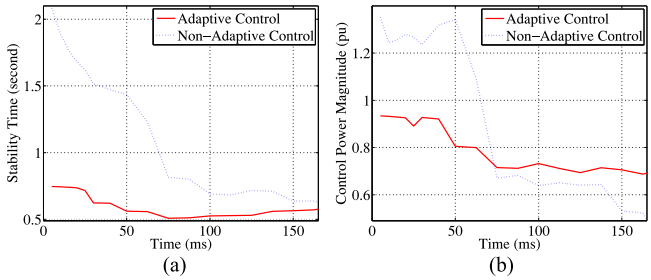

Fig. 7. Adapting the control scheme to communication latency. (a) Stability time. (b) Control power.

changes as seen in Fig. 6(d). System generators are stabilized within 1.40 s from control activation.

Fig. 7 demonstrates the impact of adapting the control design parameter to the value of communication latency; the cases of fixed $\alpha_i = D_i$ and adaptive α_i of (23) are compared. By examining the optimum value of α_i for different faults in the power system, and then, calculating a piece-wise linear relationship between the mean value of α_i versus τ, the value of the design parameter is adapted as a function of the communication latency (in millisecond) according to

$$\alpha_i(\tau_i) = \begin{cases} 32\, D_i, & \tau_i \leq 95 \\ (44 - 0.132\,\tau_i)\, D_i, & 95 < \tau_i \leq 165\,. \end{cases} \tag{23}$$

Fig. 7(a) illustrates the system stability time, and Fig. 7(b) shows the total storage power used during the stabilization process. The results show an enhanced stabilizing performance when the ESS controller adapts to the state of the cyber network. Adapting the design parameter to communication latency enhances the performance of the ESS-based control component relative to the case of nonadaptive control.

Fig. 8 demonstrates the impact of agent internal delay between controllers and actuators on the system performance. It is

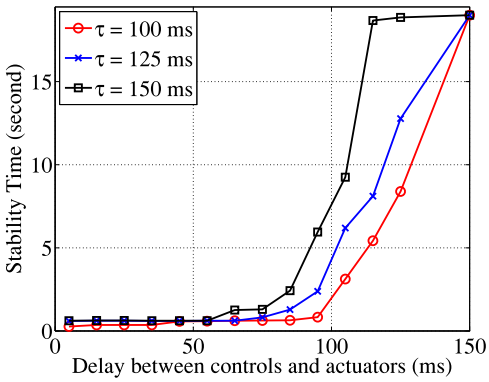

Fig. 8. Impact of delay between controls and actuators on the stability time.

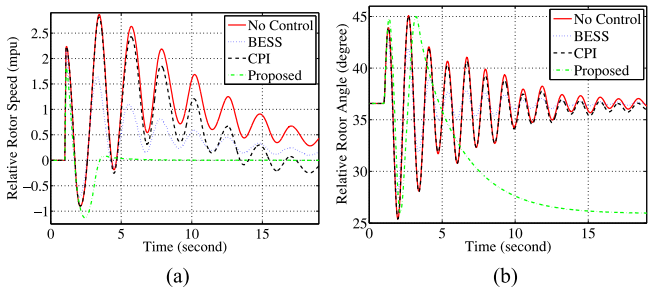

Fig. 9. Sample comparison with recent work. (a) Relative rotor speed. (b) Relative rotor angle.

observed that there is no noticeable change in the stability time for reasonable values of internal delay; however, stability time increases when this delay becomes larger. The performance degradation also intensifies when the communication latency (between agents) increases.

B. Comparison With Recent Work

The operation and control of a battery-based ESS (BESS) is optimized in [18] in order to regulate the frequency of the power system and minimize the peak frequency deviation during and after disturbances. Let Δf denote the system frequency deviation. It is proposed that no control action is required if $|\Delta f| < 0.001$ p.u., the output of the BESS is made linearly dependent on Δf if $0.001 \leq |\Delta f| < 0.004$ p.u., and the BESS absorbs or injects power in its full rated capacity if $|\Delta f| \geq 0.004$ p.u. [18]. A consensus proportional integral (CPI)-based control scheme is proposed in [16] for automatic frequency control, where the mechanical power of a synchronous generator is adjusted following a two-level control process. The generator's rotor speed is regulated against a reference speed in the first level, and the reference speed is updated in the second level. Let α_c and β_c be constants, the CPI-based control signal is calculated as [16]

$$\hat{v}_i(t) = -\alpha_c \left(\omega_i(t) - \hat{\omega}(t)\right)$$
$$\dot{\hat{\omega}}(t) = -\beta_c \frac{1}{N} \sum_{j=1}^{N} \omega_j(t) - \omega_s \,. \tag{24}$$

Along with the case of no distributed control, the proposed control scheme is compared to that of the BESS-based control in [18] and CPI control in [16] (with both α_c and $\beta_c = 2.5$) in Fig. 9 for a fault at Bus 60, where the average values of the rotor speed and angle are shown. It is observed that the proposed control scheme stabilizes the rotor speed fastest, and the rotor angle is smooth with fewer fluctuations within few seconds from the control activation time. The swing equation determines the integration relation between rotor speed and angle. For the proposed control, since the relative rotor speed converges to zero in few seconds, the rotor angle quickly becomes constant; however, for other control schemes, the rotor angle will keep changing for longer time until the relative rotor speed converges to zero.

C. Discussion

The aforementioned numerical results confirm that the proposed control framework can be useful for achieving the transient stability even with low storage capacity limits. Further, activating the v_i control scheme can slowly adjust the mechanical power of the generators to prevent continual ESS actuation. Compared to recent work, the proposed control framework achieves the transient stability rapidly by integrating both storage and mechanical power controls. The framework incorporates different reaction strategies to disturbances; it reacts to attacks on data availability by adapting the control design parameter, and the reaction strategy to threats on data integrity includes clustering.

A defense-in-depth strategy can be applied to address cyber disturbances on smart power systems, where prevention, detection, and reaction approaches are simultaneously applied at various levels for protection against these attacks. Preventative strategies aim to make attacks impossible to be carried out; such approaches include using relays and circuit breakers to prevent the propagation of severe faults [35], [36], or employing encryption and secure communication protocols against cyber intrusions [37], [38]. Further, detection strategies use system measurements and models for the identification of anomalies; such techniques are applied to detect the occurrence of a successful cyber attack [39], an unwanted system state [40], or a combination of both [41]. Finally, a reaction approach employs strategies to recover from disturbance and includes the design of robust and adaptive control schemes [42].

The proposed storage-based multiagent regulation framework can be classified as a reaction strategy to cyber disturbances. As detailed in Section IV, the proposed control scheme reacts to cyber attacks as follows.

1) *Cyber attack that delays the exchange of information*: Vary α_i as described in (17).
2) *Cyber attack that blocks the exchange of information*: Activate the local control mode of (18).
3) *Cyber attack that corrupts measurements*: Cluster the agents in control areas and apply the control of (19).

Since the proposed framework applies a reaction control strategy to recover from a disturbance, the control

framework should be accompanied with prevention and detection schemes that obstruct the impact of disturbances and identify measurement and system anomalies, respectively.

The resilience of the smart power system is enhanced in this study as the proposed storage-based multiagent regulation framework improves the power system's ability to

1) absorb a disturbance (shown in shorter times to achieve stability);
2) adapt to a disturbance (by applying controls that address limited storage or sensing capabilities);
3) recover from a disturbance (by having reactive control schemes that address cyber connectivity constraints).

Further, since the proposed framework is distributed by design, it strengthens the robustness of the control scheme to different cyber connectivity constraints. However, the distributed solution requires N control agents; thus, it might incur a higher cost compared to a centralized single-agent system.

VI. Conclusion

The aim of this paper is to lay a foundation for distributed control for the transient stability in smart grids. The proposed framework builds on the feedback linearization control theory, addresses practical constraints in energy storage and sensors, and incorporates storage-based and fast traditional power control schemes. The control scheme is adaptive in parameters and in structure to address issues such as unavailable sensor measurements, noisy measurements, unavailable sensors or storage devices, and storage with limited capacity.

Numerical results demonstrate the proposed framework's merits, and it is shown that transient stability can be achieved quickly even when the ESSs have limited capacity. Coordinating the operation of distributed control schemes of different timescales at various levels enhances power systems resilience by reducing the impact of disturbances on the transient stability. This integration also improves the controller's ability to address the practical limitations in the storage and cyber network.

Acknowledgment

The authors would like to thank Dr. A. M. Khalil at the University of Toronto for his help in simulating the power system.

References

[1] V. Güngör *et al.*, "Smart grid technologies: Communication technologies and standards," *IEEE Trans. Ind. Informat.*, vol. 7, no. 4, pp. 529–539, Nov. 2011.
[2] P. Parikh, T. Sidhu, and A. Shami, "A comprehensive investigation of wireless LAN for IEC 61850-based smart distribution substation applications," *IEEE Trans. Ind. Informat.*, vol. 9, no. 3, pp. 1466–1476, Aug. 2013.
[3] H. Tung *et al.*, "The generic design of a high-traffic advanced metering infrastructure using ZigBee," *IEEE Trans. Ind. Informat.*, vol. 10, no. 1, pp. 836–844, Feb. 2014.
[4] S. Das and T. Singh Sidhu, "Application of compressive sampling in synchrophasor data communication in WAMS," *IEEE Trans. Ind. Informat.*, vol. 10, no. 1, pp. 450–460, Feb. 2014.
[5] A. Farraj, E. Hammad, and D. Kundur, "On the use of energy storage systems and linear feedback optimal control for transient stability," *IEEE Trans. Ind. Informat.*, vol. 13, no. 4, pp. 1575–1585, Aug. 2017.
[6] W. Li, M. Ferdowsi, M. Stevic, A. Monti, and F. Ponci, "Cosimulation for smart grid communications," *IEEE Trans. Ind. Informat.*, vol. 10, no. 4, pp. 2374–2384, Nov. 2014.
[7] P. Kundur *et al.*, "Definition and classification of power system stability IEEE/CIGRE joint task force on stability terms and definitions," *IEEE Trans. Power Syst.*, vol. 19, no. 3, pp. 1387–1401, Aug. 2004.
[8] P. Fairley, "Cybersecurity at US utilities due for an upgrade," *IEEE Spectr.*, vol. 53, no. 5, pp. 11–13, May 2016.
[9] R. Langner, "Stuxnet: Dissecting a cyberwarfare weapon," *IEEE Security Privacy*, vol. 9, no. 3, pp. 49–51, May/Jun. 2011.
[10] S. Liu, X. P. Liu, and A. El Saddik, "Denial-of-service (DoS) attacks on load frequency control in smart grids," in *Proc. IEEE PES Innovative Smart Grid Technol.*, 2013, pp. 1–6.
[11] S. Cui, Z. Han, S. Kar, T. T. Kim, H. V. Poor, and A. Tajer, "Coordinated data-injection attack and detection in the smart grid: A detailed look at enriching detection solutions," *IEEE Signal Process. Mag.*, vol. 29, no. 5, pp. 106–115, Sep. 2012.
[12] F. Dörfler and S. Grammatico, "Amidst centralized and distributed frequency control in power systems," in *Proc. Amer. Control Conf.*, 2016, pp. 5909–5914.
[13] A. Vahidnia, G. Ledwich, and E. W. Palmer, "Transient stability improvement through wide-area controlled SVCs," *IEEE Trans. Power Syst.*, vol. 31, no. 4, pp. 3082–3089, Jul. 2016.
[14] M. Andreasson, D. Dimarogonas, K. Johansson, and H. Sandberg, "Distributed vs. centralized power systems frequency control," in *Proc. Eur. Control Conf.*, Jul. 2013, pp. 3524–3529.
[15] J. Wei, D. Kundur, T. Zourntos, and K. Butler-Purry, "A flocking-based paradigm for hierarchical cyber-physical smart grid modeling and control," *IEEE Trans. Smart Grid*, vol. 5, no. 6, pp. 2687–2700, Nov. 2014.
[16] M. Andreasson, D. Dimarogonas, H. Sandberg, and K. Johansson, "Distributed control of networked dynamical systems: Static feedback and integral action and consensus," *IEEE Trans. Autom. Control*, vol. 59, no. 7, pp. 1750–1764, Jul. 2014.
[17] A. Farraj, E. Hammad, and D. Kundur, "A cyber-enabled stabilizing controller for resilient smart grid systems," in *Proc. IEEE PES Conf. Innovative Smart Grid Technol.*, Feb. 2015, pp. 1–5.
[18] P. Mercier, R. Cherkaoui, and A. Oudalov, "Optimizing a battery energy storage system for frequency control application in an isolated power system," *IEEE Trans. Power Syst.*, vol. 24, no. 3, pp. 1469–1477, Aug. 2009.
[19] R. Hadidi and B. Jeyasurya, "A real-time multiagent wide-area stabilizing control framework for power system transient stability enhancement," in *Proc. IEEE Power Energy Soc. General Meeting*, 2011, pp. 1–8.
[20] P. F. Ribeiro, B. K. Johnson, M. L. Crow, A. Arsoy, and Y. Liu, "Energy storage systems for advanced power applications," *Proc. IEEE*, vol. 89, no. 12, pp. 1744–1756, Dec. 2001.
[21] J. Hossain and H. Pota, *Robust Control for Grid Voltage Stability: High Penetration of Renewable Energy*. Singapore: Springer, 2014.
[22] E. Vittal, A. Keane, J. Slootweg, and W. Kling, "Impacts of wind power on power system stability," in *Wind Power in Power Systems*, 2nd ed. New York, NY, USA: Wiley, 2012.
[23] Y. Zhang, S. Zhu, R. Sparks, and I. Green, "Impacts of solar PV generators on power system stability and voltage performance," in *Proc. IEEE Power Energy Soc. General Meeting*, San Deigo, CA, USA, Jul. 2012, pp. 1–7.
[24] A. Farraj, E. Hammad, and D. Kundur, "On the impact of cyber attacks on data integrity in storage-based transient stability Control," *IEEE Trans. Ind. Informat.*, vol. 13, no. 6, pp. 3322–3333, Dec. 2017.
[25] A. Farraj, E. Hammad, and D. Kundur, "A distributed control paradigm for smart grid to address attacks on data integrity and availability," *IEEE Trans. Signal Inf. Process. Netw.*, doi: 10.1109/TSIPN.2017.2723762.
[26] P. Sauer and M. Pai, *Power System Dynamics and Stability*. Englewood Cliffs, NJ, USA: Prentice-Hall, 1998.
[27] J. Glover, M. Sarma, and T. Overbye, *Power System Analysis & Design*, 5th ed. Cengage Learning, Stamford, CT, USA, 2011.
[28] A. Bergen and V. Vittal, *Power Systems Analysis*, 2nd ed. Englewood Cliffs, NJ, USA: Prentice-Hall, 2000.
[29] Ontario Independent Electricity System Operator (IESO), "Ontario power system restoration plan." [Online]. Available: http://www.ieso.ca, issue 11.0: 31 January 2016, Accessed on: Jul. 28, 2016.
[30] A. Farraj, E. Hammad, and D. Kundur, "A cyber-enabled stabilizing control scheme for resilient smart grid systems," *IEEE Trans. Smart Grid*, vol. 7, no. 4, pp. 1856–1865, Jul. 2016.
[31] A. Farraj, E. Hammad, and D. Kundur, "A systematic approach to delay-adaptive control design for smart grids," in *Proc. IEEE Int. Conf. Smart Grid Commun.*, Nov. 2015, pp. 768–773.
[32] E. Hammad, A. Farraj, and D. Kundur, "A resilient feedback linearization control scheme for smart grids under cyber-physical disturbances," in *Proc. IEEE PES Conf. Innovative Smart Grid Technol.*, Feb. 2015, pp. 1–5.

[33] B. Pal and B. Chaudhuri, *Robust Control in Power Systems* (Power Electronics and Power Systems Series). New York, NY, USA: Springer, 2006.
[34] A. Singh and B. Pal, "IEEE PES task force on benchmark systems for stability controls report on the 68-bus, 16-machine, 5-area system," IEEE Power and Energy Society, Tech. Rep., Dec. 2013, [Online]. Available: http://www.sel.eesc.usp.br/ieee/NETS68/New_England_New_York_68_Bus_System_study_report.pdf
[35] S. Horowitz and A. Phadke, *Power System Relaying, 4th ed.* New York, NY, USA: Wiley, 2014.
[36] B. Ravindranath and M. Chander, *Power System Protection and Switchgear*. New Age International Pvt Ltd. Publishers, New Delhi, India, 2011.
[37] T. Flick and J. Morehouse, *Securing the Smart Grid: Next Generation Power Grid Security*. Syngress, Burlington, MA, USA, 2011.
[38] W. Stallings, *Network Security Essentials: Applications and Standards*, 5th ed. Pearson, Upper Saddle River, NJ, USA, 2013.
[39] R. Berthier, W. Sanders, and H. Khurana, "Intrusion detection for advanced metering infrastructures: Requirements and architectural directions," in *Proc. IEEE Int. Conf. Smart Grid Commun.*, 2010, pp. 350–355.
[40] A. Abur and A. Expósito, *Power System State Estimation: Theory and Implementation*. Boca Raton, FL, USA: CRC Press, 2004.
[41] S. Zonouz, K. Rogers, R. Berthier, R. Bobba, W. Sanders, and T. Overbye, "SCPSE: Security-oriented cyber-physical state estimation for power grid critical infrastructures," *IEEE Trans. Smart Grid*, vol. 3, no. 4, pp. 1790–1799, Dec. 2012.
[42] P. Kundur, *Power System Stability and Control* (EPRI Power System Engineering Series). New York, NY, USA: McGraw-Hill, 1994.

Authors' photographs and biographies not available at the time of publication.